LES of Delft Jet-in-Hot Coflow burner to investigate the effect of preferential diffusion on autoignition of CH4/H2 flames

Abtahizadeh, E, de Goey, P & van Oijen, J

Original citation & hyperlink:
Abtahizadeh, E, de Goey, P & van Oijen, J 2016, 'LES of Delft Jet-in-Hot Coflow burner to investigate the effect of preferential diffusion on autoignition of CH4/H2 flames' Fuel, vol 191, no. March 2017, pp. 36-45. DOI: 10.1016/j.fuel.2016.11.054
https://dx.doi.org/10.1016/j.fuel.2016.11.054

DOI 10.1016/j.fuel.2016.11.054
ISSN 0016-2361
ESSN 1873-7153

Publisher: Elsevier

LES of Delft Jet-in-Hot Coflow burner to investigate the effect of preferential diffusion on autoignition of CH_4/H_2 flames

Ebrahim Abtahizadeh[a,*], Philip de Goey[b], Jeroen van Oijen[b]

[a] *Flow Measurement and Fluid Mechanics Research Centre, Coventry University, CV1 5FB, Coventry, United Kingdom*
[b] *Multiphase and Reactive Flows, Mechanical Engineering Department, Eindhoven University of Technology, 5600 MB Eindhoven, The Netherlands*

Abstract

This paper reports on numerical investigations of preferential diffusion effects in Large Eddy Simulation (LES) of turbulent lifted CH_4/H_2 flames. For this purpose, a combined LES and Flamelet Generated Manifolds (FGM) model is developed to simulate the Delft Jet-in-Hot Coflow (DJHC) burner. A novel type of flamelets, entitled "IML Flamelets", has been used to tabulate the chemistry. IML flamelets are capable to incorporate preferential diffusion effects in autoigniting flames. The IML technique is coupled with LES to simulate the DJHC burner with CH_4/H_2 fuels where CH_4 has been enriched with H_2 ranging from 0% to 25% of the fuel volume. The significance of this study is to illustrate complex interactions of molecular diffusion, chemistry and turbulent transport. A good agreement has been found between LES and measurements for the velocity and OH fields. It turns out that preferential diffusion has a significant influence on the lift-off height and stabilization mechanism of the lifted H_2-enriched turbulent flames. Predictions of the 0% H_2 case indicate that inclusion of preferential diffusion in the combustion model modestly affects lift-off heights. However, for 5% H_2, 10% H_2 and 25% H_2 cases, inclusion of preferential diffusion in the model affects strongly lift-off heights yielding much improved

*corresponding author
Email address: e.abtahizadeh@coventry.ac.uk (Ebrahim Abtahizadeh)

predictions compared to the unity Lewis number model. Predictions of lift-off heights and formation of ignition kernels agree very well with the measured instantaneous snapshots of OH chemiluminescence. It turns out that the combined FGM-IML approach can successfully capture main features of turbulent lifted flames such as formation of ignition kernels and stabilization mechanisms.
Keywords: Turbulent combustion, Large Eddy Simulation, Flamelet Generated Manifolds, Autoignition, Preferential diffusion, Mild combustion

1. Introduction

Combustion devices are often optimized in order to increase thermal efficiency and reduce pollutant emissions such as carbon monoxide (CO) and nitrogen oxides (NO_x). For these purposes, strategies have been developed that deploy autoignition of a fuel jet emerging in a preheated and diluted oxidizer stream. This is a type combustion often called Mild combustion or flameless oxidation [1, 2]. Stabilization of Mild combustion under intense dilution is highly sensitive to variations in fuel composition and operating conditions. Recently, addition of hydrogen to methane based fuels has been introduced in order to improve the stabilization [3, 4] and studied in some DNS studies [5, 6]. The addition of hydrogen opens a new technical challenge for numerical modeling of Mild combustion due to the complexity of autoignition under large preferential diffusion effects [7].

Experimental studies on Mild combustion have been mainly focused on a vitiated combustion regime in laboratory scale Jet-in-Hot-Coflow (JHC) burners [4, 8–10]. In the conditions of the JHC burner, a turbulent lifted flame has been observed as a result of autoignition of a fuel jet in the hot environment of burned gas. Numerical studies of the JHC burner have been mainly devoted to the development and validation of models for simulations of the lifted turbulent flames. An important issue in the numerical modeling of Mild combustion is flame stabilization which is mainly governed by autoignition. Although there are many Reynolds-Averaged Navier-Stokes (RANS) studies in this field [11–13], these un-

steady ignition events are strongly intermittent for which Large Eddy Simulation (LES) is known to provide more accurate results.

Among different approaches for LES of JHC burners, two of them have been widely and successfully used. They are either based on transported PDF methods with reduced chemistry [14, 15] or based on flamelet-based reduction techniques such as FGM (Flamelet Generated Manifold) [16], FPI (Flame prolongation of ILDM) [17] and FPV (Flamelet Progress Variable) [18]. Accuracy of predictions by transported PDF methods depends strongly on the micro-mixing model. In spite of a higher accuracy of this approach compared to presumed PDF approaches, a large set of differential equations has to be solved for an accurate description of the probability of occurrences, which results in a very large computational time. Moreover, inclusion of preferential diffusion effects in the framework of transported PDF methods is an open research question [19, 20].

Application of flamelet-based reduction techniques within LES has been reported by a number of studies for non-premixed flames assuming a unity Lewis number approximation for the combustion model [21–26]. In the context of JHC burners, Ihme et al. [23] employed the Unsteady Flamelet Progress Variable (UFPV) model for LES of the Cabra burner with CH_4/air fuel [8]. It is believed that for methane base fuels, the application of unity Lewis approximation yields accurate results. They predicted lifted turbulent flames in a good agreement with measurements. In a later study, Ihme et al. [24] simulated the HM3 case of the Adelaide burner [4] with a similar methodology but with the addition of an extra conserved scalar to account for the third surrounding air stream. Within their methodology, they used a mean scalar for temperature of the coflow and they found a good agreement with measurements of temperature, mixture fraction and concentrations of species. Due to a considerable amount of hydrogen in the HM3 case, the flame is almost attached to the burner with a structure similar to piloted flames, e.g. [27]. Application of unity Lewis number in the combustion model for such CH_4/H_2 mixtures may lead to inaccurate results. This point is investigated thoroughly in this paper.

The Delft Jet-in-Hot Coflow (DJHC) burner has been devised by Oldenhof et al. [9] with some minor differences from the Adelaide burner. They performed measurements of lifted methane flames for temperature and velocity using Coherent Anti-Stokes Raman Spectroscopy (CARS) and Laser Doppler Anemometry (LDA), respectively. Recently simulations of these lifted flames have been reported in [28–31]. In both experiments and simulations, it has been reported that the lifted flames are stabilized by autoignition in which ignition kernels form, grow and convect downstream. Later on, these experiments were extended for hydrogen containing methane mixtures by Arteaga et al. [3]. In these experiments, the methane based fuel (Dutch natural gas) has been enriched with various amounts of hydrogen ranging from 0% to 25% of fuel volume. They performed measurements of Particle Image Velocimetry (PIV) and OH chemiluminescence which revealed that addition of only a small amount of hydrogen to methane affects the flame's lift-off height and stabilization mechanism significantly. Some of these hydrogen enriched turbulent flames were lifted and others were attached to the burner. In fact, autoignition of these flames is initiated at very small mixture fractions ($\zeta < 0.02$), very close to the oxidizer stream where turbulence intensities are low [7]. In these locations, molecular diffusion becomes as important as turbulent transport in the ignition events. In this situation, prediction of autoignition might depend strongly on molecular diffusion modeling, which has to be considered carefully in the development of a numerical model. In this paper, we develop a LES model based on a combined FGM and presumed PDF model to simulate turbulent lifted flames of the DJHC burner with CH_4/H_2 fuels. The FGM model is based on the newly proposed one-dimensional Igniting Mixing Layer flamelets (IML flamelets) [32]. These flamelets have been proposed to include preferential diffusion effects in autoignition of CH_4/H_2 flames. Inclusion of heat loss in the model has been neglected in order to investigate purely preferential diffusion effects without additional modeling uncertainties.

The focus is on the prediction of autoignition in turbulent lifted flames under significant influence of preferential diffusion. In section 2, the choice of FGM technique based on

IML flamelets is briefly explained to clarify its ability to incorporate preferential diffusion effects in autoignition. Section 3 comprises a description of the LES model and numerical methodology. Computational results are presented in section 4, where LES of the lifted flames are conducted and compared with measurements to illustrate the effect of molecular diffusion and preferential diffusion. Finally, a number of conclusions are drawn.

2. Inclusion of preferential diffusion in the Manifold - IML flamelets

The studied cases contain a range of H_2 from 0% to 25% of the fuel volume which are summarized in Table 1. Modeling of combustion is performed using flamelets which are transient solution of one-dimensional laminar Igniting Mixing Layer flamelets (IML flamelets) as shown in Fig. 1. A complete description and extensive analysis of IML flamelets and their capability to predict autoignition of hydrogen enriched mixtures can be found in [32]. As a brief summary, in IML flamelets, fuel and oxidizer streams are completely unmixed at $t = 0$ s, having the shape of a step-function for all thermo-chemical properties in physical space. In these flamelets, scalar dissipation rate is close to infinity at $t = 0$ s because of the steep gradient of mixture fraction. During the time-evolution of the IML flamelets, scalar dissipation rate decreases (rapidly) due to molecular diffusion of fuel and oxidizer in which the mixture might ignite at any time. This molecular mixing process is governed by generalized Fickian and thermal diffusion without any imposed inflow momentum.

Figure 1 shows the evolution of temperature profiles in physical space for IML flamelets using detailed chemistry GRI-mech 3.0 [33] and different transport models. IML flamelets are computed using unity Lewis numbers ($Le_i = 1$) in Fig. 1a and constant non-unity Lewis numbers ($Le_i = c_i$) in Fig. 1b. Temperature profiles are plotted incrementally in time in which each time level is plotted with the same color in both graphs. It is observed that preferential diffusion affects significantly the evolution of temperature. These IML flamelets incorporate adequately simultaneous evolution of molecular mixing and chemistry

during autoignition. However, such a transient molecular mixing and chemistry cannot be accurately captured by assuming a steady-state mixing with frozen chemistry at $t = 0$ s [32], as it is a common-practice in igniting counterflow flamelets. Moreover, IML flamelets incorporate the time history of a decaying scalar dissipation rate χ_{st}, which often occurs in turbulent jet flames.

Time-dependent IML flamelets are tabulated as a function of the chosen controlling variables; mixture fraction ζ and reaction progress $\mathcal{Y}$. The mixture fraction is based on a linear combination of the mass fraction of elements H, C and O following Bilger's formulation [34]. ζ is normalized between zero and one at the oxidizer and fuel boundary, respectively. The reaction progress $\mathcal{Y}$ is selected in such a way that it contains major species and yields monotonically increasing values of $\mathcal{Y}$ with respect to time for each ζ:

$$\mathcal{Y} = \frac{\alpha_{\mathrm{O_2}}}{\mathrm{W_{O_2}}} Y_{\mathrm{O_2}} + \frac{\alpha_{\mathrm{CH_4}}}{\mathrm{W_{CH_4}}} Y_{\mathrm{CH_4}} + \frac{\alpha_{\mathrm{CO_2}}}{\mathrm{W_{CO_2}}} Y_{\mathrm{CO_2}} + \frac{\alpha_{\mathrm{H_2O}}}{\mathrm{W_{H_2O}}} Y_{\mathrm{H_2O}} + \frac{\alpha_{\mathrm{C_2H_6}}}{\mathrm{W_{C_2H_6}}} Y_{\mathrm{C_2H_6}} \qquad (1)$$

where $\mathrm{W_i}$ is molar mass of species i. α_i is chosen as $\alpha_{\mathrm{O_2}} = -0.5$, $\alpha_{\mathrm{CH_4}} = -0.5$, $\alpha_{\mathrm{CO_2}} = -0.8$, $\alpha_{\mathrm{H_2O}} = 1$ and $\alpha_{\mathrm{C_2H_6}} = -3$. Validation of the FGM database is performed in a one-dimensional configuration in which autoignition time scales of the IML flamelets are computed and compared with different chemical and transport models in Fig. 2. The IML flamelets are computed using both detailed chemistry and FGM chemistry. Two FGM databases are created from IML flamelets using detailed chemistry with either unity Lewis numbers (FGM.UL) or constant non-unity Lewis numbers (FGM.CL). A temperature rise ΔT is defined for quantification of the temporal evolution of autoignition: $\Delta T(t) = \max_\zeta \left(T(\zeta, t) - T(\zeta, 0) \right)$. Accordingly, the ignition delay τ_{ig} is defined based on the time it takes to reach the maximum temperature gradient $d(\Delta T)/dt$.

From Fig. 2, it is observed that in case of $Le_i = 1$, the difference between predicted ignition delays computed by detailed chemistry and the FGM.UL is less than 10% for all cases. This error is mainly due to numerical interpolation and grid resolution of the flamelet database which are chosen as a linear scheme and 400×400 in direction of $\zeta \times \mathcal{Y}$, respectively. Comparison of predictions by both FGM.UL and FGM.CL compared to

those of detailed chemistry with $Le_i = c_i$ reveals a significant improvement of predictions by using the FGM.CL compared to the FGM.UL. This demonstrates that using flamelets with $Le_i = c_i$ for generation of the FGM table is an essential step for accurate predictions. Remaining differences between the FGM.CL and detailed chemistry with $Le_i = c_i$, in addition to previously mentioned numerical errors, are related to the fact that preferential diffusion effects are not included in the transport equations for ζ and $\mathcal{Y}$. However, it was shown in [32] that the influence of neglecting these effects from transport equations on the predicted time scales is not significant for the studied cases. In the following section, the two FGM models, namely the FGM.UL and the FGM.CL, are applied in LES of turbulent lifted flames.

3. LES formulation and numerical details

The LES formulation of the problem is obtained from the Navier-Stokes equations which are implicitly filtered with filter width Δ_F equal to the mesh size. By application of tabulated chemistry, a set of filtered governing equations is obtained for mass, momentum, mixture fraction and reaction progress [21]:

$$\frac{\partial \bar{\rho}}{\partial t} + \frac{\partial \bar{\rho}\tilde{u}_j}{\partial x_j} = 0 \tag{2}$$

$$\frac{\partial(\bar{\rho}\tilde{u}_i)}{\partial t} + \frac{\partial(\bar{\rho}\tilde{u}_i\tilde{u}_j)}{\partial x_j} = \frac{\partial \bar{p}}{\partial x_i} + \frac{\partial}{\partial x_j}\left[(\mu_L + \mu_T)\left(\frac{\partial \tilde{u}_i}{\partial x_j} + \frac{\partial \tilde{u}_j}{\partial x_i} - \frac{2}{3}\frac{\partial \tilde{u}_k}{\partial x_k}\epsilon_{ij}\right)\right] \tag{3}$$

$$\frac{\partial(\bar{\rho}\tilde{\zeta})}{\partial t} + \frac{\partial(\bar{\rho}\tilde{u}_j\tilde{\zeta})}{\partial x_j} = \frac{\partial}{\partial x_j}\left[\left(\frac{\lambda}{c_p} + \frac{\mu_T}{Sc_T}\right)\frac{\partial \tilde{\zeta}}{\partial x_j}\right] \tag{4}$$

$$\frac{\partial(\bar{\rho}\tilde{\mathcal{Y}})}{\partial t} + \frac{\partial(\bar{\rho}\tilde{u}_j\tilde{\mathcal{Y}})}{\partial x_j} = \frac{\partial}{\partial x_j}\left[\left(\frac{\lambda}{c_p} + \frac{\mu_T}{Sc_T}\right)\frac{\partial \tilde{\mathcal{Y}}}{\partial x_j}\right] + \bar{\dot{\omega}}_{\mathcal{Y}} \tag{5}$$

Filtered quantities are specified with an over-line $\bar{\phi}$ while density-weighted filtered quantities are specified with a tilde $\widetilde{\phi} = \overline{\rho\phi}/\bar{\rho}$. Solution of the velocity components, $\tilde{\zeta}$ and $\tilde{\mathcal{Y}}$ requires values of $\bar{\rho}$, $\bar{\dot{\omega}}_{\mathcal{Y}}$ and c_p that are retrieved from the FGM table. It has to be mentioned that additional terms associated with non-unity Lewis numbers are neglected from

this formulation since, as it was shown in Fig. 2 and in [32], their influence on autoignition time scales is not considerable for the studied cases.

The turbulence/chemistry interaction is modeled through a presumed $\beta-$PDF method to statistically determine thermo-chemical variables. This model has been successfully used in previous studies of similar flames [21, 35–37]. In this method, a non-resolved filtered quantity is obtained by $\tilde{\phi} = \int\int \phi(\zeta, c) P(\zeta, c) d\zeta dc$ in which $P(\zeta, c)$ refers to the joint-PDF. In this equation, c refers to the reaction progress $\mathcal{Y}$ which is normalized between 0 and 1 at unburned and burned mixture, respectively. Complex PDF-closure techniques involve the solution of a large set of transport equations for the probability of possible realizations of the joint-PDF which requires a very large computational time. In this study, since both controlling variables ζ and c are normalized between 0 and 1, their statistical dependency is insignificant. Moreover, the high resolution of the grid (minimum cell width is 0.375 mm) used in this study makes the impact of neglecting the covariance on predictions of mean values smaller. Therefore, in order to keep the computational cost low, the statistical independence is assumed: $P(\zeta, c) = P(\zeta)P(c)$. These marginal PDFs are then modeled by a presumed β-PDF which is fully described by the first two moments: $P(\zeta) = P(\zeta; \tilde{\zeta}, \widetilde{\zeta''^2})$ and $P(c) = P(c; \tilde{c}, \widetilde{c''^2})$. This implies that the two-dimensional FGM table is extended with two additional dimensions to accommodate variances of ζ and c. The grid resolution of the PDF-integrated tables is $(101 \times 11 \times 101 \times 11)$ in the directions of $(\widetilde{\zeta} \times \widetilde{\zeta''^2} \times \widetilde{c} \times \widetilde{c''^2})$. Grid points of the variances are quadratically clustered near zero where the sensitivity of thermo-chemical variables to changes of variances are significantly larger than at high variances. To determine $\widetilde{c''^2}$ and $\widetilde{\zeta''^2}$ during turbulent flame computations, an algebraic gradient model is used, similar to that of the viscous sub-grid model:

$$\widetilde{\phi''^2} = \alpha \Delta x^2 \left(\frac{\partial \tilde{\phi}}{\partial x_j} \right)^2 . \tag{6}$$

The value of $\alpha = 1/12$ based on the Taylor-expansion of the gradient term in Eq. (6). Although the chosen sub-grid models are not the most accurate available models in the

literature, they do not have a large influence on the predictions due to the present high resolution grid in which the minimum cell width is $\Delta x = 0.375$ mm resolving approximately 90% of the turbulence energy spectrum.

μ_L and λ in Eqs. (2-5) are calculated based on simplified formulations following [16, 38]

$$\mu_L = 1.67 \times 10^{-8} (T/298)^{0.51} c_p \qquad (\text{kg m}^{-1}\ \text{s}^{-1}), \tag{7}$$

$$\lambda = 2.58 \times 10^{-5} (T/298)^{0.69} c_p \qquad (\text{W m}^{-1}\ \text{K}^{-1}). \tag{8}$$

The eddy-viscosity μ_T is calculated using a model proposed by Vreman [39] to close nonlinear terms in equations for u, ζ and $\mathcal{Y}$. In this model, μ_T is determined by an eddy-viscosity/eddy-diffusivity closure approach in which the eddy-diffusivity μ_T/Sc_T is obtained using a fixed turbulent Schmidt number, $Sc_T = 0.4$. Equations (7,8) use the PDF-averaged temperature in the manifold to compute and store μ_L and λ in the look-up table.

The LES model is applied to the DJHC burner, which has been fully described in [3, 9]. In this burner, the fuel jet is ignited by the hot coflow of burned gas with low levels of oxygen. The injection of the fuel jet takes place through a fuel pipe ($D = 4.5$ mm) with a peak velocity of 32 m/s resulting in a jet exit Reynolds number of approximately 4500. The hot coflow stream enters the domain with a bulk velocity of 3 m/s through an annulus of 82.8 millimeter diameter. The coflow stream consists of the combustion products of a ring of premixed flames on the secondary burner that are mixed and cooled with the injected ambient air on both sides of the secondary burner. Because of this cooling mechanism, the coflow stream has a non-uniform profile of temperature. In this study, a mean value for temperature and composition of the coflow is used to avoid the need for an extra scalar in our combustion model. This choice is further discussed in subsection 4.2.

The computational domain is a Cartesian grid of size $86 \times 86 \times 250$ mm with the largest dimension in the stream-wise direction. The grid resolution is chosen as fine as our computational resources allow, in order to minimize numerical and modeling er-

rors (cf. [40]). There are approximately 7.5 million grid cells that are distributed non-equidistantly, stretching from the fuel injection point in all three directions. The minimum cell width is 0.375 mm which is less than the laser probe size that has been used to obtain the experimental data. Velocity components, ζ and normalized mixture fraction c have homogeneous Neumann boundary conditions at the side planes and at the outflow-plane. For pressure, a Dirichlet ($p = p_0$) boundary condition is applied at the side planes in x and y direction while a Neumann boundary condition is applied at the inflow and outflow plane. To account for the fluctuations in the inflow velocity of the fuel and oxidizer in experiments, mean and RMS values of inflow are reproduced using a filtered random noise generator [21]. In this generator, random numbers are applied to each velocity component at the inflow plane at every time-step. All the velocity components are then spatially filtered using a box-filter with size $\Delta_F = D/4$ and subsequently with a temporal filter of $\Delta_T = \Delta t/4$ yielding nearly isotropic homogeneous turbulence at the inflow.

The numerical implementation to solve the mathematical model adopts a variable density approach, similar to low-Mach number methods, which involves the solution of a Poisson equation for the pressure. A standard finite-volume method is used with second order central differencing on a staggered Cartesian mesh. Temporal discretization is based on a third-order Adams-Bashforth for the convective terms and a forward Euler for the viscous terms and source terms. This hybrid time-stepping method provides more stability than pure Adams-Bashforth scheme or pure forward Euler. A constant time step of $\Delta t = 0.4\ \mu s$ is used for all simulations in order to keep the CFL-number sufficiently low. The scalar equations for ζ and c are discretized using third order Van Leer's MUSCLE scheme, which is Total Variation Diminishing (TVD), for convective terms while the viscous terms are discretized second order central differencing. Computations are conducted using an in-house LES solver for which more details can be found in [21]. This code adopts a multi-grid implementation to solve the Poisson's equation which has been extensively described in [21]. Parallelization has been performed using a combined MPI and OpenMP

protocol on a multi-block platform.

4. Results

4.1. Flow field statistics

Flow field statistics have been calculated using ensemble-averaging of density-weighted fields for 10 flow-through times of the fuel jet. Comparison of predicted mean stream-wise velocities $\{\widetilde{w}\}$ with measurements at several heights is shown in Fig. 3. It is observed that $\{\widetilde{w}\}$ of the fuel jet in the middle of the domain, is significantly larger than $\{\widetilde{w}\}$ of the coflow which creates velocity fluctuations and turbulence in the shear layer between these two streams. The computed RMS values of stream-wise and span-wise velocity components, $\{\widetilde{w''^2}\}^{1/2}$ and $\{\widetilde{u''^2}\}^{1/2}$, are compared with measurements in Fig. 4. The RMS values which indicates standard deviation are calculated from

$$\{\widetilde{w''^2}\}^{1/2} = \left[\sum_{i=1}^{n} \frac{\widetilde{w}_i^2}{n} - \left(\sum_{i=1}^{n} \frac{\widetilde{w}_i}{n}\right)^2\right]^{1/2} \tag{9}$$

where i and n refer to the number of instant and total number of instants, respectively.

It is observed that there is a good agreement between computations and experiments for the velocity components and turbulent kinetic energy. There are some discrepancies for $\{\widetilde{w''^2}\}^{1/2}$ near the peak values (30 mm $<$ Z $<$ 60 mm) which are located in the transition region of the fuel jet from laminar to turbulence. In such regions, the accuracy of predictions become highly dependent on Sub-Grid Scale (SGS) modeling and therefore, Smagorinsky model might not provide excellent accuracy. $\{\widetilde{u''^2}\}^{1/2}$ agrees well at most radial locations. In particular, the predictions near the shear layer, where ignition kernels are formed, are promising. It turns out that application of the random noise generator reproduces successfully the inflow turbulence of the experiments. Overall, the mixing field is predicted reasonably well for autoignition predictions.

4.2. Influence of preferential diffusion on the lift-off height

Figure 6 shows instantaneous snapshots of the filtered OH concentration $\widetilde{Y}_{\mathrm{OH}}$ which is obtained from the LES of Case D00H$_2$ with the FGM.CL model. It is observed that at $t = 96$ ms, a $\widetilde{Y}_{\mathrm{OH}}$ kernel is formed at approximately $Z = 200$ mm. Subsequently, this kernel grows and convects downstream at $t = 100$ ms and $t = 104$ ms. This mechanism, which is repeated in subsequent times, governs stabilization of the flame. Further downstream, these kernels further grow and ignite the surrounding mixture. It is apparent that this flame is stabilized by autoignition in which ignition kernels are formed, grow and convect downstream corresponding to experimental observations by Oldenhof et al. [9]. These ignition events are formed at the lean side ($\zeta < \zeta_{st}$=0.0178) very close to the oxidizer stream where molecular diffusion is comparable with turbulence transport (eddy viscosity).

In order to further clarify such a distinct formation of ignition kernels in 3D, iso-surfaces of $\widetilde{\zeta}_{st} = 0.0178$ and $\widetilde{\mathcal{Y}} = 2.9$ are shown in Fig. 7. These values of $\widetilde{\zeta}$ and $\widetilde{\mathcal{Y}}$ correspond to a temperature rise of 50 K from the manifold which is an indicator of autoignition. Considering this, it is seen from Fig. 7 that an ignition kernel is formed at a specific axial distance from the jet exit at $t = 137.6$ ms. Afterwards, this kernel grows and ignites the downstream mixture at later times. A similar trend occurs repeatedly for other kernels in time.

In order to investigate the influence of hydrogen addition on such a flame structure, a snapshot of $\widetilde{Y}_{\mathrm{OH}}$ is plotted for Case D10H$_2$ is shown in Fig. 8. In this case, OH forms right after the jet exit which indicates a totally different structure than the one observed for Case D00H$_2$. The structure of Case D10H$_2$ corresponds to experimental observations of OH chemiluminescence by Arteaga et al. [3]. This structure resembles a diffusion flame structure which is stabilized by an edge flame, in clear contrast with the autoignition structure of Case D00H$_2$. Further analysis of the flame stabilization for the studied cases is discussed in subsection 4.3.

Figure 9 shows the time-averaged $\{\widetilde{Y}_{\mathrm{OH}}\}$ distributions obtained from the statistics of

approximately 10 flow-through times of the fuel jet for all cases and models. The $\{\widetilde{Y}_{\mathrm{OH}}\}$ fields are shown here in order to compare with the measurements of OH chemiluminescence. In Fig. 9, it is observed that computations with the FGM.UL result in approximately the same lift-off height for cases D00H_2, D05H_2 and D10H_2. However, computations with the FGM.CL indicate a significant change of the lift-off height among these cases especially between cases D00H_2 and D05H_2. For Case D25H_2, the FGM.CL yields an attached flame to the jet exit. These observations indicate that preferential diffusion has a strong influence on the stabilization height and mechanism of the studied flames. It has to be mentioned that for cases with significant ignition and extinction (e.g. Case D00H_2), the $\{\widetilde{Y}_{\mathrm{OH}}\}$ field is highly intermittent and therefore, the time-averaged field is not very smooth. However, cases with a more steady flame structure (e.g. Case D25H_2) indicate a smooth field. Regardless of the case, time-averaged fields of both controlling variables ζ and $\mathcal{Y}$ are statistically converged and smooth for all cases (not shown here). These flame stabilization mechanisms are analyzed and discussed in detail in subsection 4.3.

The time-averaged plots in Fig. 9 are compared with the measurements represented by red lines which show the measured 50% probability of OH chemiluminescence (more details can be found in [3]). By comparison of the $\{\widetilde{Y}_{\mathrm{OH}}\}$ plots with the red lines, it appears that, except for Case D00H_2, the trend in lift-off heights are captured very well with the FGM.CL model in contrast to the FGM.UL model which predicts considerably higher lifted flames. This observation demonstrates that inclusion of preferential diffusion in the combustion model is essential for hydrogen enriched cases. In cases D10H_2 and D25H_2, formation of OH is predicted at somewhat smaller heights than the red lines. This can be explained considering the fact that our computational model does not take into account heat loss effects leading to a uniform distribution of the inflow temperature at the coflow side. Such a uniform distribution results in a higher temperature, compared to measurements, in close vicinity of the jet exit. This condition for the cases with small lift-off heights (cases D10H_2 and D25H_2) leads to a faster ignition and consequently lower lift-off heights. It should be

mentioned that in experiments, there is heat loss from the coflow to the cooled fuel pipe upstream of the computational domain of the current study, leading to a non-uniform mean temperature profile as shown in [9]. The heat loss can be added to our combustion model by inclusion of at least one extra scalar. However, such an extension is not pursued here in order to exclude additional modeling uncertainties and focus on preferential diffusion effects. Inclusion of the heat loss has been performed in several previous studies [24, 30] but in combination with preferential diffusion effects, it remains as a future research.

It is interesting to compare lift-off heights of these turbulent flames with the ignition delays of IML flamelets that were shown in Fig. 2. It is clear that the lift-off heights follow a very similar trend to the ignition delays. In particular, for Case D00H_2, the ignition delay computed using the FGM.CL model is larger than that of the FGM.UL model. This trend corresponds very well with the higher lift-off height of the computed flame (Case D00H_2) using the FGM.CL model compared to the one using the FGM.UL model. Accordingly, the significant change of ignition delay between Case D00H_2 and D05H_2 (by application of the FGM.CL) comply well with the predicted lift-off height of these cases by using these FGM models. This behavior is explained considering that, as mentioned earlier, ignition of these flames is initiated at very low mixture fractions ($\zeta < \zeta_{st}$=0.0178) very close to the oxidizer side. In this region, turbulent structures in the fuel stream can hardly intrude the ignition kernels at the most reactive mixture fraction ζ_{MR} [41] which induces that molecular diffusion is comparable with turbulence transport. In this condition, it is expected that these turbulent flames behave very similar to laminar flames. This behavior is also related to the Reynolds number of these cases which is not relatively very high (Re = 4500).

From Figs. 2 and 9, it is observed that Case D00H_2 follows a different trend when preferential diffusion is included. Application of the FGM.CL to Case D00H_2 leads to a larger ignition delay and consequently a higher lift-off height in contrast to the other cases. This can be explained considering that in Case D00H_2, hydrogen is not initially present in the fuel. During the pre-ignition phase, chain branching reactions form some

H_2 molecules and H radicals. These species diffuse away from ζ_{MR} due to the preferential diffusion. This leads to a lower reactivity at ζ_{MR} and consequently an increased ignition delay and lift-off height. However, for other cases, hydrogen is initially present in the fuel. Due to preferential diffusion effects, diffusion of hydrogen from the fuel to ζ_{MR} is enhanced leading to a much higher reactivity at ζ_{MR} and eventually a decreased ignition delay and lift-off height. This is also the reason that the ignition delay and lift-off height decreases significantly from Case D00H_2 to Case D05H_2.

4.3. Stabilization mechanism of the lifted flames

In the previous subsection, based on instantaneous $\widetilde{Y}_{OH}$ distributions, a clear formation of ignition kernels has been observed for Case D00H_2. Similar behavior was observed for Case D05H_2 (but not shown here). However, the stabilization mechanism of Case D10H_2 and D25H_2 in which the fuel jet immediately burns after injection into the domain, is not completely clear. In this subsection, we make further clarifications on the stabilization mechanisms of the flames and assess them whether they are manily based on autoignition or self-propagation. For this purpose, first, we remove autoignition chemistry from the FGM look-up table by setting $\bar{\dot{\omega}}_{\mathcal{Y}} = 0$ at the beginning of reaction progress, $\widetilde{c} = 0$. Afterwards, we apply such a look-up table to a LES initiated from an already burning solution. Finally, we analyze results to realize whether the flames are stabilized by autoignition or a self-propagating flame structure.

This procedure has been applied to all cases and it is shown for Case D05H_2 in Fig. 10. In this figure, the left picture shows the initial field and the next two pictures show the progress of the LES simulation. It is seen that for this case, the flame is gradually washed out when the FGM table does not include autoignition chemistry. This clearly demonstrates that flame is mainly stabilized by autoignition. We tested the same procedure for Case D00H_2 and observed similar behavior (not shown here). However, the two other cases (D10H_2 and D25H_2) remained burning with the same lift-off height. These observations demonstrate that autoignition is the main stabilization mechanism of Case D00H_2 and

$D05H_2$, while the two other cases are stabilized by flame propagation. Furthermore, it turns out that the IML approach is not only capable of prediction of autoignition but it also predicts flame propagation with a very good accuracy.

5. Conclusions

A numerical model has been developed to study the influence of preferential diffusion on the lift-off height and stabilization mechanism of turbulent lifted flames in a hot coflow. For this purpose, IML flamelets have been employed to create a flamelet database and to handle preferential diffusion effects in the model. A four dimensional flamelet database ($\widetilde{\zeta} \times \widetilde{\zeta''^2} \times \widetilde{\mathcal{Y}} \times \widetilde{\mathcal{Y}''^2}$) has been generated for each studied case in which variances are included with β-PDF approximation. LES of turbulent lifted flames has been performed using FGM.UL and FGM.CL models. The DJHC burner has been chosen as a test case which has been fed with a range of CH_4/H_2 mixtures. Comparison of the mixing field between computations and experiments indicates a good agreement. It is found that the influence of preferential diffusion on the stabilization height of the 0% H_2 case is not significant. In this case, both FGM.UL and FGM.CL models yield a reasonable prediction of the lift-off height compared to measurements. However, preferential diffusion affects strongly the lift-off height of hydrogen enriched cases, especially the 5% H_2 case compared to the 0% H_2 case. This trend is not captured using the FGM.UL model, which yields approximately the same lift-off height for 0% H_2, 5% H_2 and 10% H_2 cases. Comparison of all studied cases with the measured OH chemiluminescence demonstrates the necessity of inclusion of preferential diffusion in the combustion model (FGM.CL) for hydrogen containing cases (5% H_2, 10% H_2 and 25% H_2). Further analysis of computational results reveal that the 0% H_2 and 5% H_2 cases are stabilized by autoignition in which there are distinct ignition kernels which form, grow and convect downstream. On the other hand, 10% H_2 and 25% H_2 cases are stabilized by a propagation mechanism without ignition kernels. These observations are in a good agreement with the measured instantaneous

snapshots of OH chemiluminescence. Therefore, it is concluded that hydrogen enrichment leads to a significant change in the lift-off height and stabilization mechanism of the lifted turbulent flames under studied conditions. There is an under-prediction of lift-off height for the 10% H_2 and 25% H_2 cases using the FGM.CL model which can be explained due to the neglecting of heat loss. As a future study, predictions can be further improved by the extension of proposed model with at least one extra scalar in order to include heat loss effects.

Acknowledgments

The authors gratefully acknowledge the financial support of the Dutch Technology Foundation (STW) under project No. 10414.

[1] Cavaliere A, De Joannon M. Mild Combustion. Prog Energy Combust Sci 2004;30(4):329–66.

[2] Wunning JA, Wunning JG. Flameless oxidation to reduce thermal NO-formation. Prog Energy Combust Sci 1997;23(1):81–94.

[3] Arteaga LDA, Tummers MJ, Van Veen EH, Roekaerts DJEM. Effect of hydrogen addition on the structure of natural-gas jet-in-hot-coflow flames. Proc Combust Inst 2015;35(3):3557-64.

[4] Dally BB, Karpetis AN, Barlow RS. Structure of turbulent non-premixed jet flames in a diluted hot coflow. Proc Combust Inst 2002;29(1):1147-54.

[5] Göktolga MU, van Oijen JA, de Goey LPH. 3D DNS of MILD combustion: A detailed analysis of heat loss effects, preferential diffusion, and flame formation mechanisms. Fuel 2015;159(1):784–95.

[6] Dinesh KKJR, Jiang X, van Oijen JA, Direct numerical simulation of non-premixed syn-gas burning with detailed chemistry. Fuel 2013;107:343–55.

[7] Van Oijen JA. Direct numerical simulation of autoigniting mixing layers in MILD combustion. Proc Combust Inst 2013;34(1):1163-71.

[8] Cabra R, Myhrvold T, Chen JY, Dibble RW, Karpetis AN, Barlow RS. Simultaneous laser Raman-Rayleigh-LIF measurements and numerical modeling results of a lifted turbulent H2/N2 jet flame in a vitiated coflow. Proc Combust Inst 2002;29(2):1881-88.

[9] Oldenhof E, Tummers MJ, Van Veen EH, Roekaerts DJEM. Ignition kernel formation and lift-off behaviour of jet-in-hot-coflow flames. Combust Flame 2010;157(6):1167-78.

[10] Abtahizadeh SE, Sepman A, Hernández-Pérez F, Van Oijen JA, Mokhov A, De Goey LPH, Levinsky H. Numerical and experimental investigations on the influence of preheating and dilution on transition of laminar coflow diffusion flames to Mild combustion regime. Combust Flame 2013;160(11):2359-74.

[11] Kim SH, Huh KY, Dally BB. Conditional moment closure modeling of turbulent nonpremixed combustion in diluted hot coflow. Proc Combust Inst 2005;30(1):751–57.

[12] Parente A, Malik MR, Contino F, Cuoci A, Dally BB, Extension of the Eddy Dissipation Concept for turbulence/chemistry interactions to MILD combustion, Fuel 2016;163:98–111.

[13] Mardani A, Tabejamaat S, Ghamari M. Numerical study of influence of molecular diffusion in the Mild combustion regime. Combust Theory Modelling, 2010:747-774.

[14] Pope SB. PDF methods for turbulent reactive flows. Prog Energ Combust Sci 1985;11:119-92.

[15] Haworth DC, Progress in probability density function methods for turbulent reacting flows. Prog Energ Combust Sci 2010;36(2):168-259.

[16] Van Oijen JA, De Goey LPH. Modelling of premixed laminar flames using flamelet-generated manifolds. Combust Sci and Tech 2000;161(1):113-37.

[17] Gicquel O, Darabiha N, Thevenin. Laminar premixed hydrogen/air counterflow flame simulations using flame prolongation of ILDM with differential diffusion, Proc Combust Inst 2000;28(2):1901–8.

[18] Ihme M, Cha CM, Pitsch H. Prediction of local extinction and re-ignition effects in non-premixed turbulent combustion using a flamelet/progress variable approach. Proc Combust Inst 2005;30(1):793-800.

[19] Wang H, Kim K. Effect of molecular transport on PDF modeling of turbulent non-premixed flames. Proc Combus Inst 2015;35(2):1137-45.

[20] Tirunagari RR, Pope SB. LES/PDF for premixed combustion in the DNS limit. Combust Theory Modelling, 2016:834-865.

[21] Vreman AW, Albrecht BA, Van Oijen JA, De Goey LPH, Bastiaans RJM, Premixed and non-premixed generated manifolds in large-eddy simulation of Sandia flame D and F. Combust Flame 2008;153(3):394-416.

[22] Bekdemir C, Somers LMT, De Goey LPH, Tillou J, Angelberger C. Predicting diesel combustion characteristics with Large-Eddy Simulations including tabulated chemical kinetics. Proc Combust Inst 2013;34(2):3067-74.

[23] Ihme M, See YC. Prediction of autoignition in a lifted methane/air flame using an unsteady flamelet/progress variable model. Combust Flame 2010;157(10):1850-62.

[24] Ihme M, See YC, LES flamelet modeling of a three-stream MILD combustor: Analysis of flame sensitivity to scalar inflow conditions. Proc Combust Inst 2011;33(1):1309-17.

[25] Kempf A, Flemming F, Janicka J. Investigation of length scales, scalar dissipation, and flame orientation in a piloted diffusion flame by LES. Proc Combust Inst 2005;30(1):557-65.

[26] Dinesh KKJR, Jiang X, Malalasekera W, Odedra A. Large eddy simulation of fuel variability and flame dynamics of hydrogen-enriched nonpremixed flames. Fuel Process Technol 2013;107:2–13.

[27] Barlow RS, Frank JH, Effects of turbulence on species mass fractions in methane/air jet flames, Proc Combust Inst 1998;27(1):1087-95.

[28] Labahn JW, Dovizio D, Devaud CB. Numerical simulation of the Delft-Jet-in-Hot-Coflow (DJHC) flame using Conditional Source-term Estimation. Proc Combust Inst 2015;35(3):3547-55.

[29] Labahn JW, Devaud CB, Large Eddy Simulations (LES) including Conditional Source-term Estimation (CSE) applied to two Delft-Jet-in-Hot-Coflow (DJHC) flames. Combust Flame 2016;164:68-84.

[30] Sarras G, Mahmoudi Y, Arteaga Mendez LD, Van Veen EH, Tummers MJ, Roekaerts DJEM. Modeling of Turbulent Natural Gas and Biogas Flames of the Delft Jet-in-Hot-Coflow Burner: Effects of Coflow Temperature, Fuel Temperature and Fuel Composition on the Flame Lift-Off Height. Flow Turb Combust 2014;93(4):607–35.

[31] Bhaya R, De A, Yadav R. Large Eddy Simulation of Mild Combustion Using PDF-Based Turbulence–Chemistry Interaction Models. Combust Theory Modelling, 2014:1138-1165.

[32] Abtahizadeh SE, de Goey LPH, van Oijen JA, Development of a novel flamelet-based model to include preferential diffusion effects in autoignition of CH4/H2 flames. Combust Flame 2015;162(11):4358–69

[33] Smith GP, Golden DM, Frenklach M, Moriarty NW, Eiteneer B, Goldenberg M, Bowman CT, Hanson RK, Song S, Gardiner WC, Lissianski VV, Qin Z, GRI-Mech 3.0, available at <http://www.me.berkeley.edu/gri_mech/>.

[34] Bilger RW, The structure of turbulent nonpremixed flames. Proc Combust Inst 1989;22:475-88.

[35] Ramaekers WJS, Van Oijen JA, De Goey LPH. Stratified turbulent Bunsen flames: flame surface analysis and flame surface density modelling. Combust Theor Model 2012;16(6):943-75.

[36] Mukhopadhyay S, van Oijen JA, de Goey LPH. A comparative study of presumed PDFs for premixed turbulent combustion modeling based on progress variable and its variance, Fuel 2015;159:728–40.

[37] Mukhopadhyay S, Bastiaans RJM, van Oijen JA, de Goey LPH. Analysis of a filtered flamelet approach for coarse DNS of premixed turbulent combustion, Fuel 2015;144:388–99.

[38] Smooke MD, Reduced Kinetic Mechanisms and Asymptotic Approximations for Methane-Air Flames, Lecture Notes in Physics, Springer, Berlin, 1991, vol. 384.

[39] Vreman AW, Bastiaans RJM, Geurts BJ. A similarity subgrid model for premixed turbulent combustion. Flow Turb Combust 2009;82:233-48.

[40] Egüz U, Ayyapureddi S, Bekdemir C, Somers B, de Goey P, Manifold resolution study of the FGM method for an igniting diesel spray, Fuel 2013;113:228–38

[41] Mastorakos E. Ignition of turbulent non-premixed flames. Prog Energy Combust Sci 2009;35(1):57-97.

Table 1: Reference inflow values of the fuel stream for the different cases. The oxidizer stream has the same values for all cases: $T = 1437$ K, $X_{O_2} = 0.0485$, $X_{H_2O} = 0.1452$, $X_{CO_2} = 0.0727$, $X_{N_2} = 0.7336$. ζ_{st} is the stoichiometric mixture fraction.

Case	T(K)	X_{H_2}	X_{CH_4}	$X_{C_2H_6}$	X_{N_2}	ζ_{st}
D00H_2	448	0.00	0.813	0.037	0.15	0.0178
D05H_2	448	0.05	0.763	0.037	0.15	0.0179
D10H_2	448	0.10	0.713	0.037	0.15	0.0180
D25H_2	448	0.25	0.563	0.037	0.15	0.0183

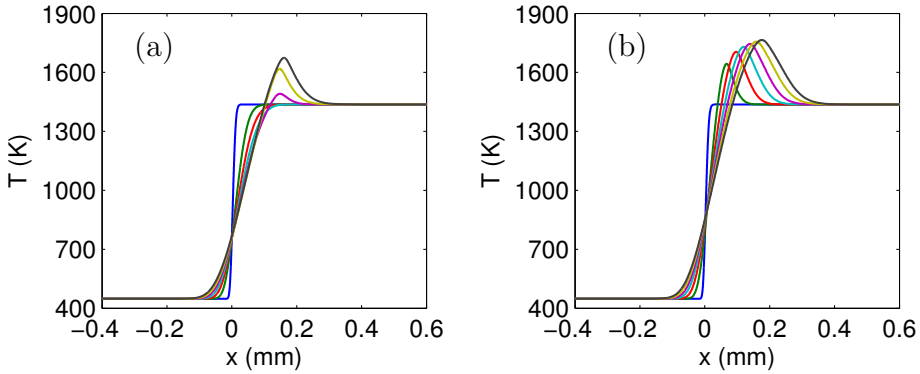

Figure 1: Evolution of temperature for (a) IML flamelets with $Le_i = 1$, (b) IML flamelets with $Le_i = c_i$, (c) ICF flamelets with $Le_i = 1$ and (d) ICF flamelets with $Le_i = c_i$. Flamelets are plotted at t = 0, 0.5, 1, ..., 3 ms.

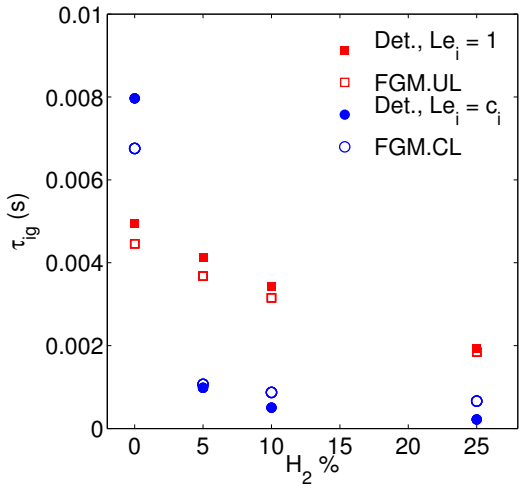

Figure 2: Computed τ_{ig} for IML flamelets using both detailed and FGM chemistry, Cases D00H$_2$, D05H$_2$, D10H$_2$ and D25H$_2$. Transport models used for computations are unity Lewis numbers ($Le_i = 1$) and constant non-unity Lewis numbers ($Le_i = c_i$).

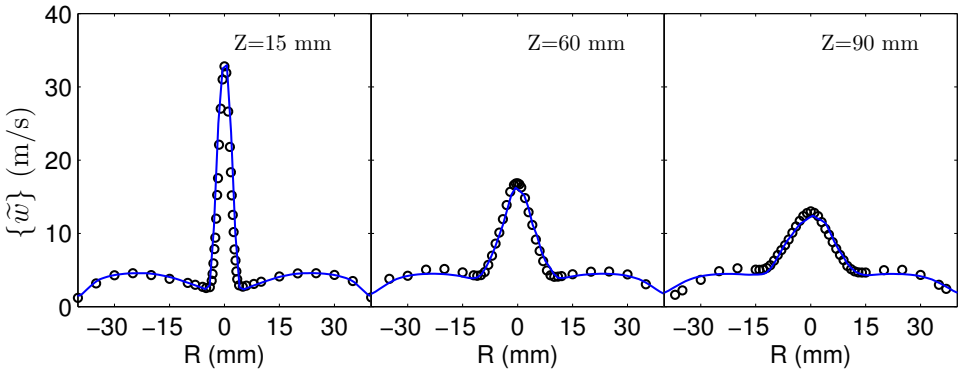

Figure 3: Radial profiles of (lines) computed and (circles) measured [9] mean stream-wise velocity at heights Z = 15, 60 and 90 for Case D00H$_2$.

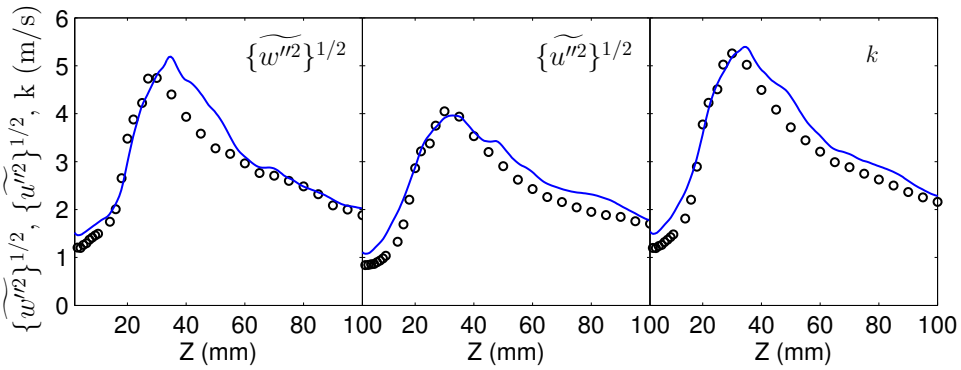

Figure 4: Centerline profiles of (lines) computed and (circles) measured [9] RMS of stream-wise velocity, RMS of span-wise velocity and turbulence kinetic energy ($k = 1/2(\{\widetilde{w''^2}\}^{1/2} + 2\{\widetilde{u''^2}\}^{1/2})$) for Case D00H$_2$.

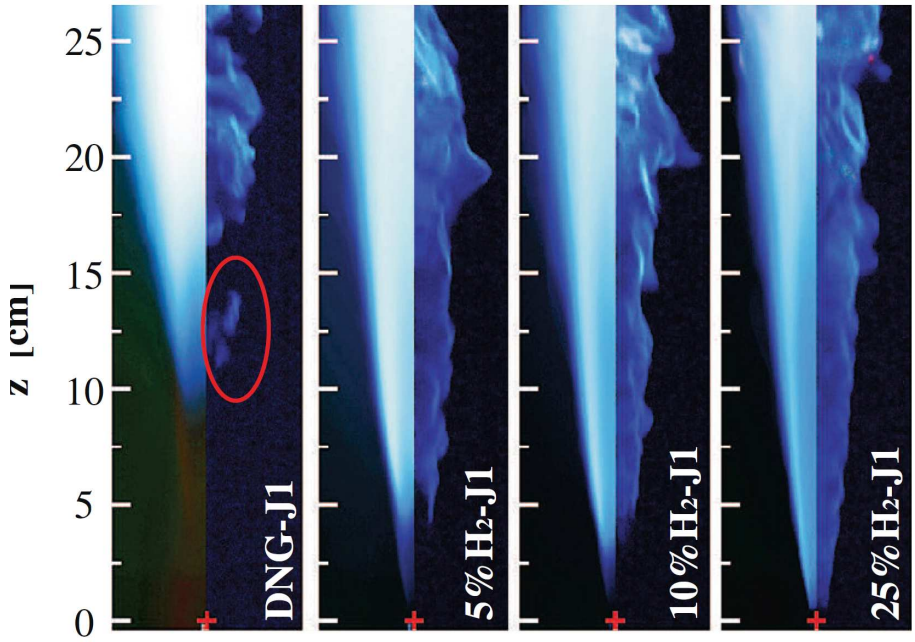

Figure 5: Reprinted images of the flames base by Arteaga et al. [3] at (left) a long exposure time of 1 s and (right) a short exposure time of 0.5 ms. The red ellipse points out an autoignition kernel and the red crosses denote the fuel pipe exit. The image width is approximately 8 cm.

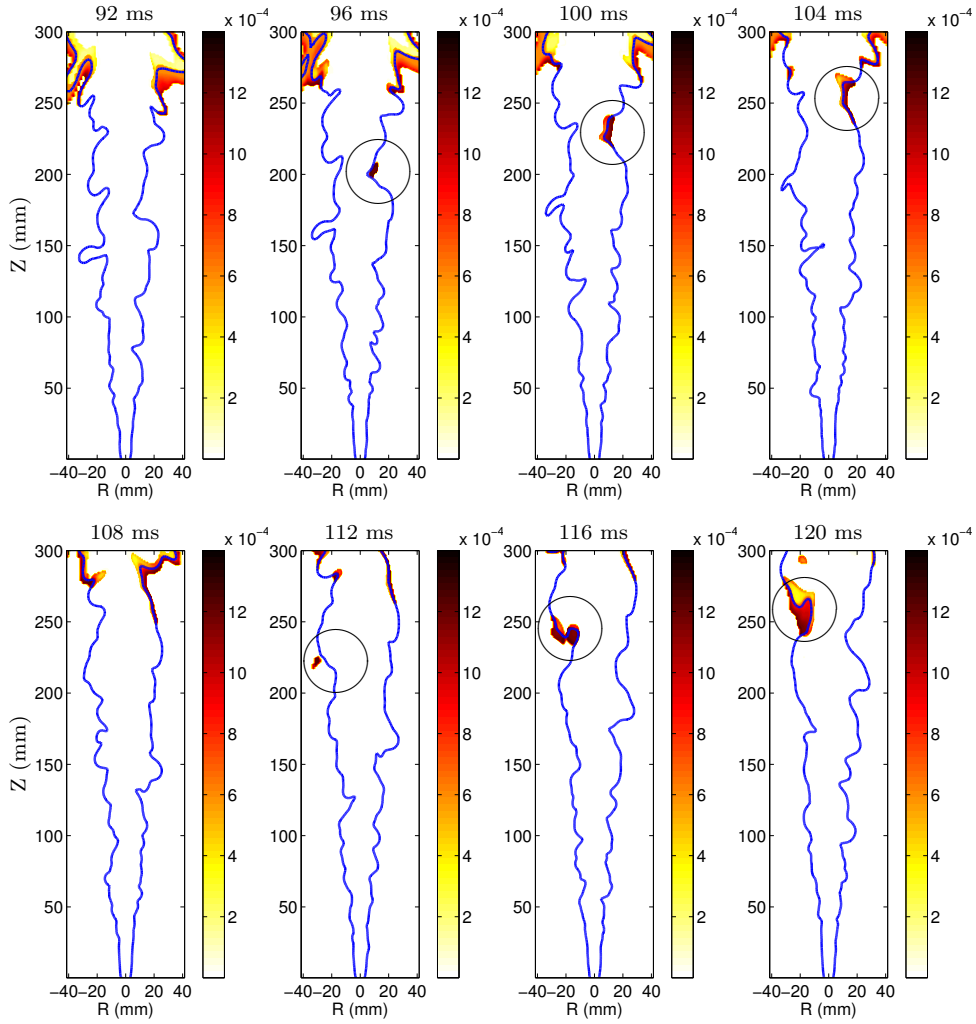

Figure 6: Computed instantaneous snapshots of $\widetilde{Y}_{\mathrm{OH}}$ using the FGM.CL model for Case D00H$_2$. Blue lines indicate stoichiometric mixture fraction ζ_{st}.

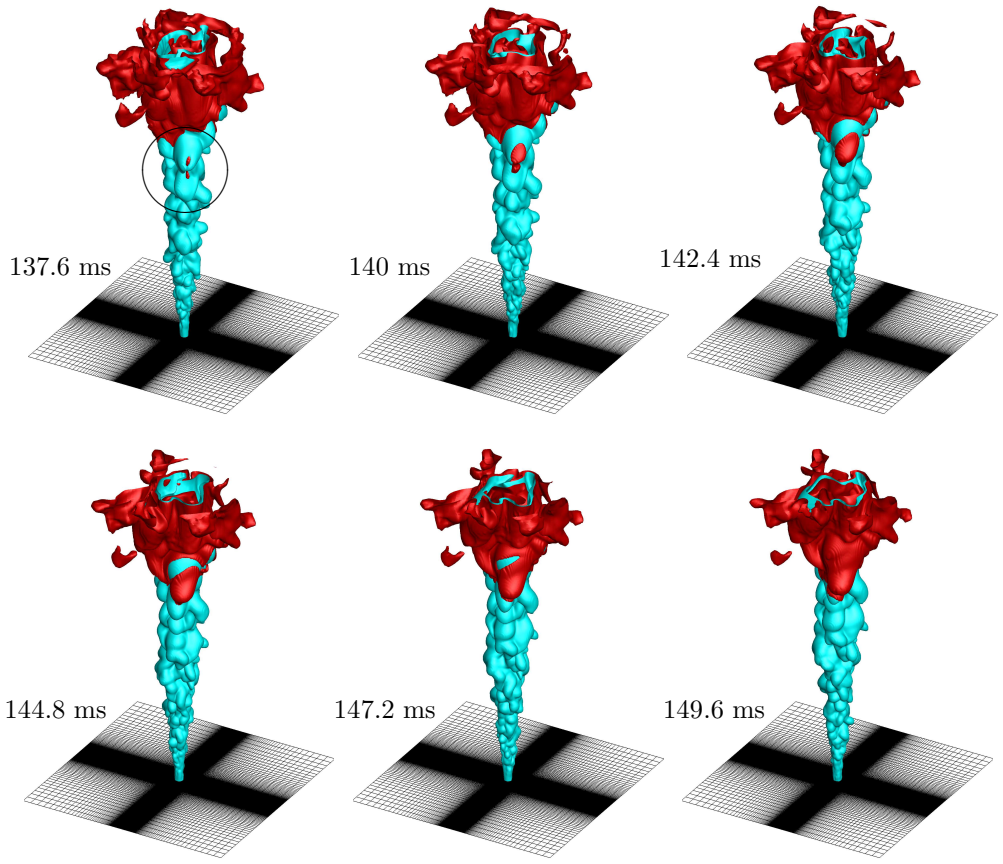

Figure 7: Computed instantaneous iso-surfaces of $\widetilde{\zeta}_{st} = 0.0178$ (blue) and $\widetilde{\mathcal{Y}} = 2.9$ (red) using the FGM.CL model for Case D00H$_2$.

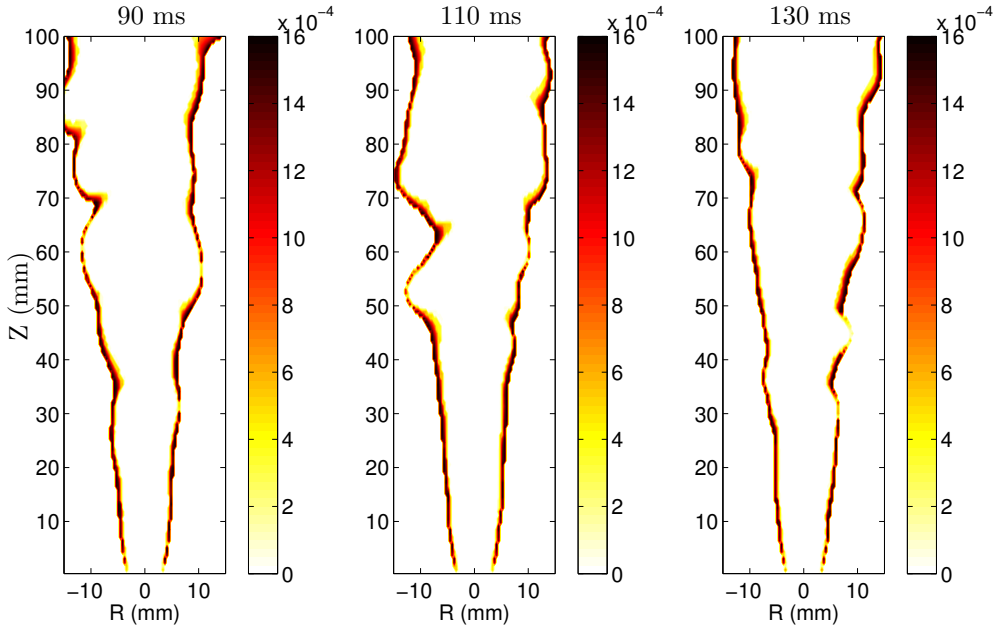

Figure 8: Computed instantaneous snapshot of $\widetilde{Y}_{\mathrm{OH}}$ using the FGM.CL model for Case D10H$_2$.

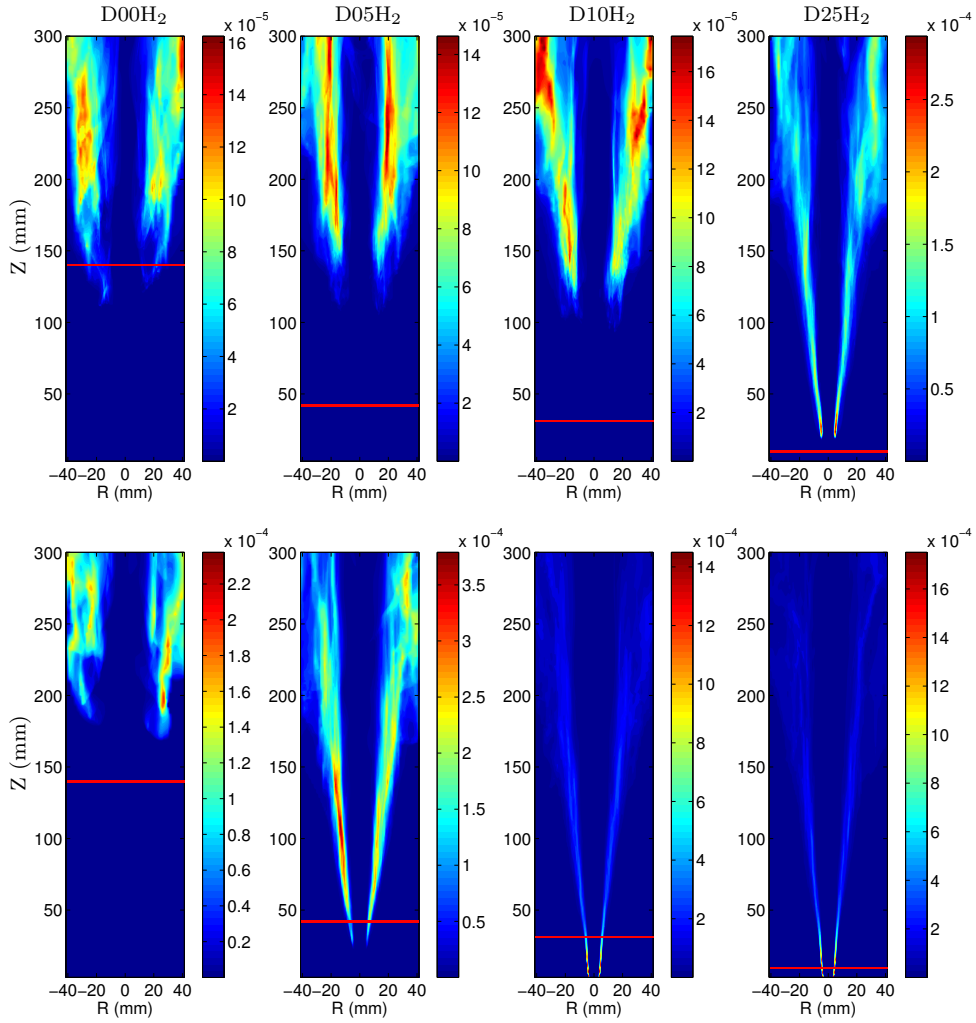

Figure 9: $\{\widetilde{Y}_{\mathrm{OH}}\}$ for all cases (from left to right $D00H_2$, $D05H_2$, $D10H_2$ and $D25H_2$). Computations with (top) the FGM.UL model and (bottom) the FGM.CL model. Red lines correspond to 50% probability of OH chemiluminescence by measurements [3].

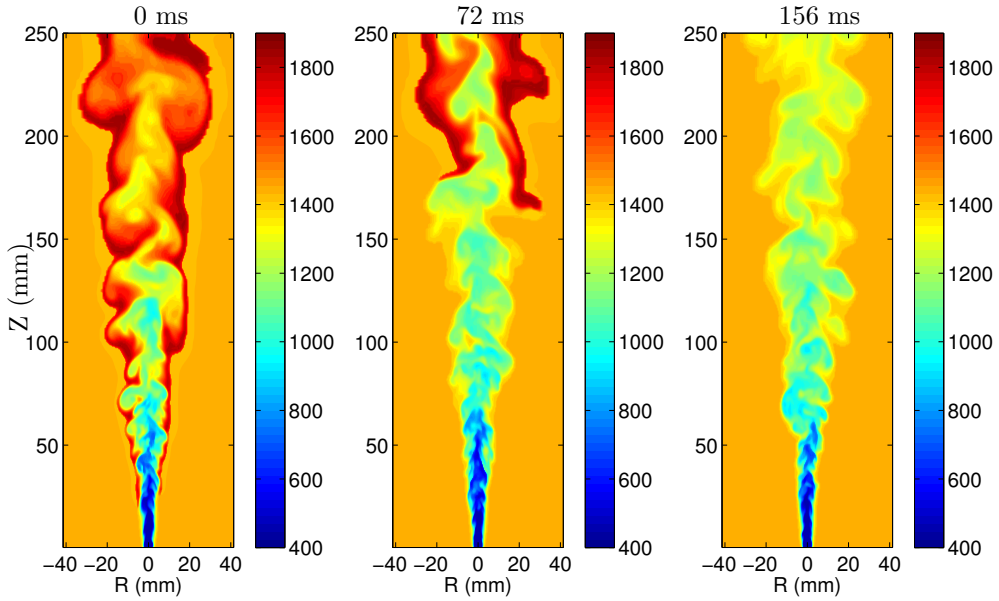

Figure 10: Computed instantaneous distributions of $\widetilde{T}$ using the FGM.CL model without ignition chemistry for Case D05H_2.